

# Design of A Single Antenna With Tunable In-Band RCS Null Through Load Impedance Control

Binchao Zhang, Weidong Hu, Fan Yang, Shenheng Xu, and Maokun Li

**Abstract-** Reducing the in-band and co-polarization radar cross section (RCS) of antennas has been a widely concerned problem. However, most of works focus on RCS reduction of antenna arrays, and there are few studies for a single antenna. Therefore, this letter presents a method to control the null of the in-band RCS by changing the load impedance of the antenna, so as to effectively reduce the RCS at particular directions. First, the relationship between the null position and the load impedance is calculated by analyzing the in-band scattering field of the antenna. Second, the load impedance of the traditional patch antenna is controlled by cascading an open-circuit stub of different lengths on the feeding line. Then, the null tuning of the in-band RCS is realized. Simulated and measured results show that the designed patch antenna can tune the null of in-band RCS from 0° to 60°. Thus, the in-band RCS is effectively reduced under the premise that the radiation performance is basically unchanged.

**Index Terms-** Antennas, in-band, load impedance, RCS reduction, RCS null tunable.

## I INTRODUCTION

With the rapid development of radar detection technology, the stealth performance of equipment platform has become an important guarantee for its survival capability. Through stealth coating and shape modification, the radar cross section (RCS) of equipment can be effectively reduced. As a result, the RCS caused by antenna scattering becomes the main contribution to the overall RCS of the equipment. Therefore, it is necessary to reduce the in-band and out-of-band RCS of various antennas.

In past research, the out-of-band RCS of antennas has been effectively reduced, whether it is monostatic RCS or bistatic RCS. Common methods include the use of artificial magnetic conductors (AMC) [1], broadband absorbers [2]-[3], and various multifunctional integrated metasurfaces [4]-[7]. However, research on the reduction of in-band and co-polarized RCS of antennas is relatively limited, as it often leads to the deterioration of radiation performance. In the published literatures, three common methods are used to reduce the in-band RCS of antennas. The earliest method involves optimizing the shape of the antenna, such as removing a portion of metal from antennas [8], application of bionics [9], and design of fractal patterns [10]. Another popular method is to tune the scattering field of the antenna by using additional circuits at the feeding port [11]-[15], which can create a favorable phenomenon that the antenna mode scattering field and the structural mode scattering field cancel each other, and thus construct the minimum RCS. The third method is to integrate the antenna and the metasurface, so that the radiation performance of the antenna and the RCS reduction ability of the metasurface are organically combined and do not affect each other, and then achieve both in-band radiation and stealth [16]-[20].

Furthermore, by loading digital components into antenna elements, the reconfigurable characteristics of the antenna's

scattering field can be achieved [21]-[24]. By changing the state of the digital element on each antenna unit, the scattering field can be artificially manipulated to achieve multi-function RCS control, such as scattering field beamforming, scattering pattern null control, etc., so as to adapt to the radar network detection system. However, all these studies require a certain aperture and a certain number of antenna elements, so that the RCS can be regulated by controlling the amplitudes and phases of the scattered electric field of each element. To the best of the authors' knowledge, there has no research on tuning in-band RCS null for a single antenna.

To fill this technological gap, this letter presents a design method to control the null of the in-band RCS by controlling the load impedance of the antenna. First, the relationship between the null position and the load impedance is analyzed and calculated to give the load impedance value corresponding to each null position. Second, each required load impedance is obtained by optimizing the position and width of the cascaded open-circuit stub. Thus, the tunable in-band RCS null is realized without affect the antenna's radiation performance.

## II THEORY AND DESIGN

### A Theory

According to the literature [25], the in-band scattering field  $\vec{E}^s$  of the antenna typically comprises two parts. The first part is the structural mode scattering field  $\vec{E}^{ss}$ , which is independent of the load impedance of the antenna, and equals the scattering field when the antenna is terminated with a matched load. The second part is the antenna mode scattering field  $\vec{E}^{as}$ , which varies with the load impedance of the antenna. The expression are as follows

$$\vec{E}^s = \vec{E}^{as} + \vec{E}^{ss}, \quad (1)$$

$$\vec{E}^{as}(Z_L) = \frac{\Gamma_L}{1 - \Gamma_A \Gamma_L} \frac{1 - \Gamma_A^2}{2} [\vec{E}^s(\infty) - \vec{E}^s(0)], \quad (2)$$

$$\vec{E}^{ss}(Z_A) = \frac{(1 - \Gamma_A)\vec{E}^s(\infty) + (1 + \Gamma_A)\vec{E}^s(0)}{2}. \quad (3)$$

Here,  $\vec{E}^s(\infty)$  and  $\vec{E}^s(0)$  respectively represent the scattering fields when the antenna is terminated with open and short loads.  $\Gamma_L$  and  $\Gamma_A$  are the terminal and the antenna reflection coefficients, respectively. Their definitions are as follows:

$$\Gamma_L = \frac{Z_L - Z_c}{Z_L + Z_c}, \quad \Gamma_A = \frac{Z_A - Z_c}{Z_A + Z_c}, \quad (4)$$

where  $Z_L$ ,  $Z_A$  and  $Z_c$  represent the terminated load impedance, antenna input impedance, and characteristic impedance of the transmission line, respectively. By substituting equations (2) to (4) into (1), it can be further simplified to

$$\vec{E}^s(Z_L) = \frac{Z_L}{Z_A + Z_L} \vec{E}^s(\infty) + \frac{Z_A}{Z_A + Z_L} \vec{E}^s(0). \quad (5)$$

From equation (5), it can be understood that the amplitude and phase of the in-band and co-polarized scattering field can be controlled by adjusting the terminal load impedance  $Z_L$ . If the RCS null is at  $\theta_{Null}$ , that is  $\vec{E}^s(Z_L)|_{\theta=\theta_{Null}} = 0$ , the terminated load impedance must satisfy

$$Z_L|_{\theta=\theta_{Null}} = -Z_A * \frac{\vec{E}^s(0)|_{\theta=\theta_{Null}}}{\vec{E}^s(\infty)|_{\theta=\theta_{Null}}}. \quad (6)$$

The following two conclusions can be drawn from formula (6): (1) When  $\theta_{Null} = 0^\circ$ , the minimum monostatic RCS is obtained.

(2) By choosing different  $\theta_{Null}$ , the in-band RCS null is controlled, thereby reducing the RCS near the direction  $\theta_{Null}$ . On the other hand, the change of load impedance  $Z_L$  will inevitably lead to the deterioration of antenna impedance matching. Therefore, the variation range of  $Z_L$  must be limited to meet the impedance matching performance, such as  $|S_{11}| < -10$  dB.

## B Antenna Design

A traditional patch antenna is used to verify the method of tuning RCS null by controlling the load impedance, whose structure is shown in Fig. 1. The dielectric layers are Rogers RO3003 with a permittivity of 3, and their thicknesses are  $t_1 = 2$  mm and  $t_2 = 1$  mm, respectively. The antenna is designed to operate at a frequency of  $f_0 = 2$  GHz, hence the dimensions of the patch are  $L_x = 45$  mm and  $L_y = 41.5$  mm, with a feed line width of  $w = 2.5$  mm and a via-hole radius of  $r = 0.5$  mm. The size of the antenna is  $P = 70$ mm, which is slightly small than half-wavelength.

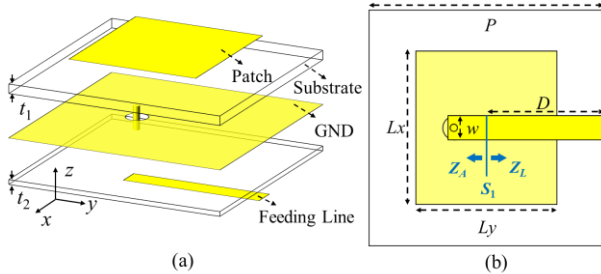


Fig. 1 Schematic diagram of the antenna, (a) front view and (b) bottom view.

Using the HFSS simulation software, the designed patch antenna is simulated with open boundary conditions and a plane wave excitation. Then, the open-load scattered field  $\vec{E}^s(\infty)$  and the short load scattered field  $\vec{E}^s(0)$  of the antenna is obtained. For the radiation simulation, a discrete port excitation is set at the reference plane  $S_1$  (without loss of generality, the distance  $D$  from the feed line terminal to  $S_1$  is 23mm), thereby obtaining the antenna impedance  $Z_A = 45.58 - j6.69$ . Thus, according to equation (6), the required load impedance to adjust the RCS null  $\theta_{Null}$  from  $0^\circ$  to  $90^\circ$  at 2 GHz for this patch antenna can be calculated, as shown in Fig. 2. Moreover, the antenna input impedance  $Z_A$  and the calculated  $|S_{11}| = |(Z_L - Z_A)/(Z_L + Z_A)|$  are presented in Fig. 2. It is seen that under the restriction of  $|S_{11}| < -10$  dB, the

RCS zero varies in the range of  $\pm 60^\circ$ , as shown in the gray area.

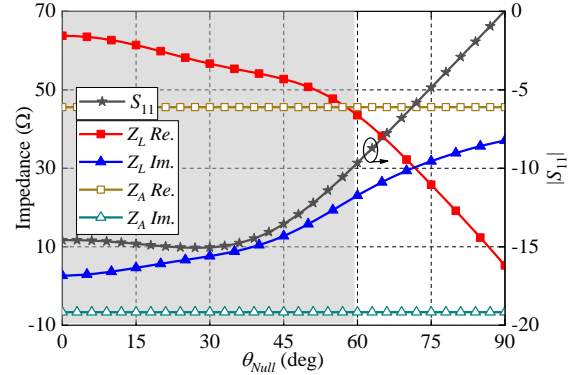


Fig. 2 Required load impedance for tuning the RCS nulls, the input impedance  $Z_A$  and the calculated  $S_{11}$ .

## C Load Impedance Control

As shown in Fig. 3, the load impedance  $Z_L$  is controlled by cascading open-circuit stub of different lengths  $L_s$  at a distance  $d_s$  from the terminal on the feeding line. Based on transmission line theory, the load impedance  $Z_L$  is

$$Z_L = Z_C \frac{Z'_L + jZ_C \tan \sqrt{\epsilon_r} \beta (D - d_s)}{Z_C + jZ'_L \tan \sqrt{\epsilon_r} \beta (D - d_s)}, \quad (7)$$

$$Z'_L = Z_C \frac{R + jZ_C \tan \sqrt{\epsilon_r} \beta d_s}{Z_C + jR \tan \sqrt{\epsilon_r} \beta d_s} // -j \frac{Z_{Cs}}{\tan \sqrt{\epsilon_r} \beta L_s}, \quad (8)$$

where  $Z_C$  and  $Z_{Cs}$  are the characteristic impedances of the feeding line and the cascaded open-circuit stub, respectively, which depends on the line widths  $w$  and  $w_s$ . The effective dielectric constant of the dielectric substrate is  $\epsilon_r$ , and  $\beta = 2\pi/\lambda_0$  is the propagation constant, with  $R$  being  $50\Omega$ . Observing equations (7) and (8), it is seen that the real part of the load impedance  $Z_L$  is mainly determined by  $Z_C$ , while the imaginary part can be controlled by the parameter  $d_s$ .

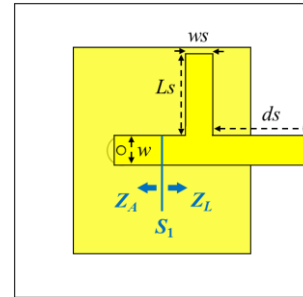


Fig. 3 Schematic diagram of the antenna with controllable load impedance.

As shown in Fig. 4(a), the distance  $d_s$  of the cascaded open-circuit stub from the terminal has a significant impact on the imaginary part of the load impedance and a slightly impact on the real part. Increasing  $d_s$  can effectively decrease the imaginary part of the load impedance. Fig. 4(b) shows the relationship between the feed line width  $w$  and the load impedance. It is observed that increasing  $w$  can effectively reduce the real part of the load impedance, while the imaginary part remains relatively unchanged. Therefore, for the required load impedance  $Z_L|_{\theta=\theta_{Null}}$ , one can first adjust the imaginary part of the impedance by changing  $d_s$ , and then fit the real part by

changing  $w$  to obtain the desired load impedance.

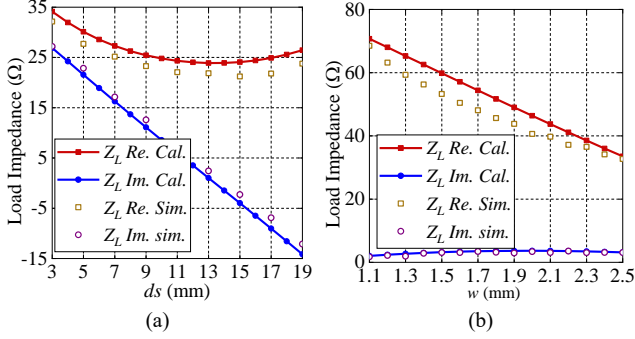


Fig. 4. Comparison of simulation and calculation results for load impedance with varying parameters: (a) different  $d_s$ , with  $L_s = 10$  mm,  $w = w_s = 2.5$  mm, (b) different  $w$ , with  $L_s = 5$  mm,  $w_s = 2.5$  mm,  $d_s = 10$  mm.

Table I Corresponding parameters for the required load impedance

$\theta_{null}$	Desired $Z_L(\Omega)$	$w$	$d_s$	$L_s$	$w_s$	Sim. $Z_L(\Omega)$
$0^\circ$	$63.8 + j2.6$	1.4	9.5	4	2.5	$63.9 + j2.8$
$15^\circ$	$61.4 + j4.6$	1.45	8.8	4	2.5	$62.7 + j4.9$
$30^\circ$	$56.7 + j7.6$	1.65	7.5	4	2.5	$57.2 + j7.6$
$45^\circ$	$52.7 + j12.7$	1.9	4	4	2.5	$53.9 + j12.4$
$60^\circ$	$43.5 + j23.1$	1.1	8.3	10	2.5	$42.6 + j23.2$

#### D RCS Null Tuning

Following the aforementioned method, by adjusting  $d_s$  and  $w$ , parameter combinations corresponding to the RCS nulls at  $\theta_{null} = (0^\circ, 15^\circ, 30^\circ, 45^\circ, 60^\circ)$  are obtained, as shown in Table I. It is seen that the simulated load impedance has little deviation from the desired values. Using these parameter combinations, the simulated RCS nulls are obtained and compared with the theoretical calculated values, as shown in Fig. 5(a), and the results agree well. Here, the calculated results involve substituting the simulated  $Z_L$  from Table I into formula (5) to calculate the scattering electric field, and then calculating the RCS using the formula

$$\sigma = \lim_R 4\pi R^2 |\vec{E}^s|^2 / |\vec{E}^i|^2, \quad (9)$$

where the distance  $R = 1$  m and the incident electric field strength  $|\vec{E}^i| = 1$  V/m. In addition, Fig. 5(b) shows the reflection coefficients and realized gains of the antenna when tuning the RCS nulls. It is seen that the antenna's  $S_{11}$  remains below -10 dB within the operating band, and the realized gain is also stable, which indicates that the radiation performance is largely unaffected. Additionally, when the RCS null is at  $60^\circ$ ,  $S_{11}$  approaches -10 dB, suggesting that the upper limit for null tuning is around  $60^\circ$ .

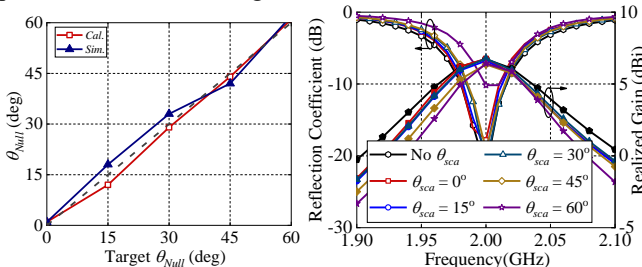


Fig. 5. (a) Comparison of simulated and calculated RCS nulls, (b) Simulated reflection coefficients and gains of different RCS nulls.

The calculated and simulated bistatic RCS patterns when the nulls at  $\theta_{null} = (0^\circ, 15^\circ, 30^\circ, 45^\circ, 60^\circ)$  are presented in Fig. 6, which are in good agreement. From these results, it is concluded that the null of the in-band RCS can be flexibly controlled by changing the load impedance. Moreover, compared to the conjugate matched load, the monostatic RCS is significantly reduced when the null changes from  $0^\circ$  to  $45^\circ$ . In particular, when null is set to  $0^\circ$ , the monostatic RCS is more than 30 dB lower than conjugated matched load. Therefore, by adjusting the load impedance, the RCS at the null position and the monostatic RCS can be reduced simultaneously.

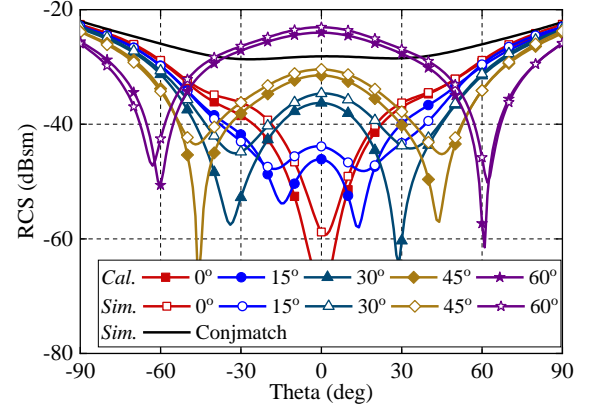


Fig. 6. RCS pattern with different nulls at  $\theta_{null} = (0^\circ, 15^\circ, 30^\circ, 45^\circ, 60^\circ)$  and also with conjugate matched load.

#### IV. FABRICATION AND MEASUREMENT

Five patch antennas for the nulls at  $\theta_{null} = (0^\circ, 15^\circ, 30^\circ, 45^\circ, 60^\circ)$  are fabricated to verify the proposed design method, as shown in Fig. 7. These five prototypes have the same radiation patch but the different loads. It should be noted that compared to the simulation structure, the fabricated prototypes need to introduce the SMA and the patch for grounding. Thus, the parameters in Table I need to be re-optimized, and the optimized parameters are listed in Table II.

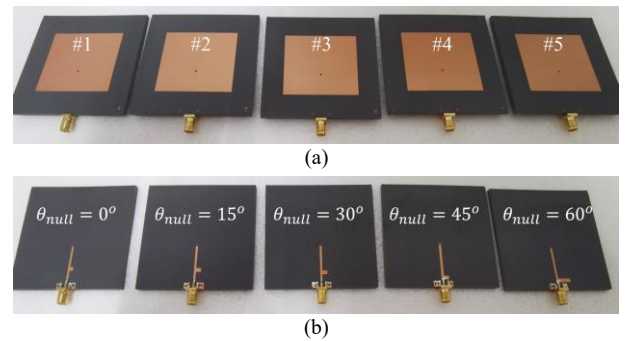


Fig. 7. Fabrication prototypes, (a) top view and (b) bottom view.

Table II Optimized parameters for the different RCS nulls.

Ant. Order	$\theta_{null}$	$w$	$d_s$	$L_s$	$w_s$
#1	$0^\circ$	1.4	12.8	2	2.5
#2	$15^\circ$	1.3	12	3	2.5
#3	$30^\circ$	1.4	10	3	2.5
#4	$45^\circ$	1.6	6	3	2.5
#5	$60^\circ$	1.5	6	8	2.5

Then, the fabricated prototypes are placed in the anechoic chamber to measure the radiation and scattering performance,

as shown in Fig. 8. The designed antennas operate as a transmitting antenna when the radiation performance is measured, as shown in Fig. 8(a). When the scattering performance is measured, the antennas under measured are terminated with a matching load to as a scatterer. A transmitting antenna, denoted as Tx, serves to normally irradiate the designed antenna, while the receiving antenna, Rx, rotates around to measure the scattering pattern, as shown in Fig. 8(b). The distance  $D$  between the designed antenna and the Tx antenna is 500 mm.

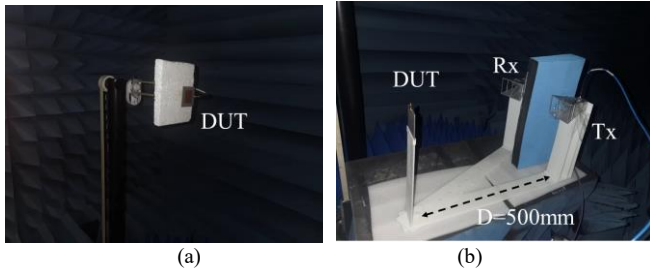


Fig. 8. Measurement setup for (a) radiation and (b) scattering performance.

The measured radiation results are presented in Fig. 9. Compared with the simulated results, the measured reflection coefficients and realized gains are agreed well. The slight difference is due to the errors caused by machining and welding. Moreover, the measured normalized radiation patterns under different RCS nulls are shown in Fig. 9(b). It is found that the radiation patterns are basically stable when the null of RCS changes. In general, the radiation performance of antenna is relatively stable when regulating the in-band and co-polarization RCS null, which is in line with the design objectives.

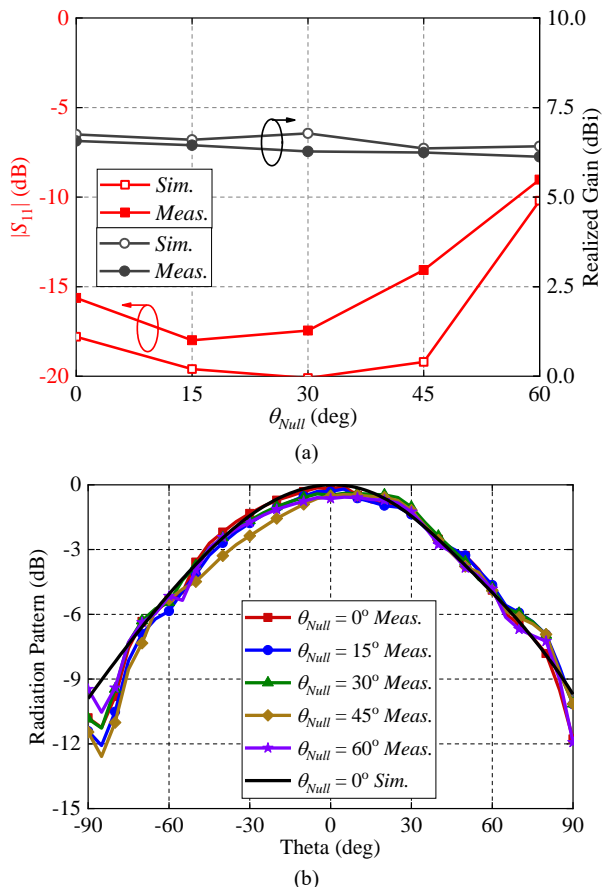


Fig. 9. Simulated and measured radiation performance under different RCS

nulls, (a) reflection coefficients and realized gains, (b) normalized radiation patterns.

When assessing the scattering performance, it should be mentioned that due to the limitations of the arch frame, the range of the scattering pattern is confined within  $15^\circ$  to  $60^\circ$ , and thus the RCS nulls at  $30^\circ$  and  $45^\circ$  are measured. The simulated and measured normalized RCS patterns under different nulls are presented in Fig. 10. The measured results show that the designed antennas can tuning the in-band and co-polarization RCS null, although the measured nulls are shifted compared to the simulated result. The reason is that the welding of SMA will inevitably introduces additional parasitic parameters, which will enlarge the load impedance, so that the nulls will shift to a lower angle.

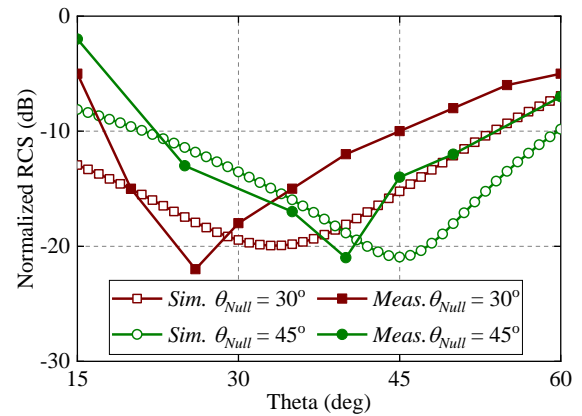


Fig. 10. Simulated and measured normalized RCS patterns under different nulls.

Compared with the existing work on controlling the in-band RCS of antennas, the innovative contribution of this letter lies in the fact that a single antenna can realize RCS controlling without the necessary of forming an array. Based on the theoretical analysis, by changing the load impedance of the antenna, the in-band RCS null of the single antenna can be regulated. On this basis, the monostatic RCS and also the RCS in the null directions of the antenna can be effectively reduced.

## V. CONCLUSION

A design method to control the null of the RCS by controlling the load impedance is proposed in this letter. Through analyzing and calculating the relationship between the null and the load impedance, each required null can be realized by optimizing the position and width of the cascaded open-circuit stub. Thus, the tunable in-band RCS null is realized without affect the antenna's radiation performance. This design method can provide an effective solution for the reduction of bistatic RCS of a single antenna.

## REFERENCES

- [1]. D. Sang, Q. Chen, L. Ding, M. Guo, and Y. Fu, "Design of checkerboard AMC structure for wideband RCS reduction," *IEEE Trans. Antennas Propag.*, vol. 67, no. 4, pp. 2604–2612, Apr. 2019.
- [2]. B. Zhang, C. Jin, and Z. Shen, "Low-profile broadband absorber based on multimode resistor-embedded metallic strips," *IEEE Trans. Microw. Theory Techn.*, vol. 68, no. 3, pp. 835–843, Mar. 2020.
- [3]. Y. Li, P. Gu, Z. He, Z. Cao, J. Cao, K. Leung, and D. Ding, "An ultra-wideband multilayer absorber using an equivalent circuit-based approach," *IEEE Trans. Antennas Propag.*, vol. 70, pp. 11911–11921, Dec. 2022.

- [4]. B. Zhang, C. Jin, L. Yin, Q. Lv, P. Zhang, and B. Tian, "Diffusive-reflective metasurface with dual independent reflection bands for RCS reduction," *IEEE Antennas Wireless Propag. Lett.*, vol. 21, no. 3, pp. 635-639, Mar. 2022.
- [5]. B. Zhang, C. Jin, and Z. Shen, "Absorptive frequency-selective reflector based on bent metallic strip embedded with chip-resistor," *IEEE Trans. Antennas Propag.*, vol. 68, no. 7, pp. 5736-5741, Jul. 2020.
- [6]. Y. Yu, W. Yu, G. Xie, J. Tong, and G. Q. Luo, "Wideband RCS reduction of slot array antenna utilizing 3-D absorptive frequency-selective structure," *IEEE Antennas Wireless Propag. Lett.*, vol. 21, pp. 64-68, Jan. 2022.
- [7]. C. Jin, B. Zhang, L. Yin, Q. Lv, L. Kong, and L. Li, "Integrated low-profile low radar cross section circularly polarized dipole antenna array," *IEEE Trans. Antennas Propag.*, vol. 69, no. 12, pp. 8461-8469, Dec. 2021.
- [8]. N. Rajesh, K. Malathi, S. Raju, V. A. Kumar, S. D. R. Prasath, and M. G. N. Alsath, "Design of Vivaldi antenna with wideband radar cross section reduction," *IEEE Trans. Antennas Propag.*, vol. 65, no. 4, pp. 2102-2105, Apr. 2017.
- [9]. W. Jiang, Y. Liu, S. Gong, and T. Hong, "Application of bionics in antenna radar cross section reduction," *IEEE Antennas Wireless Propag. Lett.*, vol. 8, pp. 1275-1278, 2009.
- [10]. Y. B. Thakare and Rajkumar, "Design of fractal patch antenna for size and radar cross section reduction," *IEEE Microw. Antennas Propag.*, vol. 4, no. 2, pp. 175-181, Feb. 2010.
- [11]. Z. Zhang, F. Yang, Y. Chen, S. W. Qu, J. Hu, and S. Yang, "In-band scattering and radiation tradeoff of broadband phased arrays based on scattering-matrix approach," *IEEE Trans. Antennas Propag.*, vol. 69, no. 11, pp. 7486-7496, Nov. 2021.
- [12]. N. Nakamoto, T. Takahashi, T. Fukasawa, N. Yoneda, and H. Miyashita, "RCS synthesis of array antenna with circulators and phase shifters and measurement method for deterministic RCS reduction," *IEEE Trans. Antennas Propag.*, vol. 69, no. 1, pp. 135-145, Jan. 2021.
- [13]. P. Li, S. Qu, S. Yang, and J. Hu, "In-band SCS reduction of microstrip phased array based on impedance matching network," *IEEE Trans. Antennas Propag.*, vol. 70, no. 1, pp. 330-340, Jan. 2022.
- [14]. Z. Zhang, S. Yang, F. Yang, Y. Chen, S. Qu, and J. Hu, "Ultralow scattering design of wideband conformal arrays based on optimally loaded resistors," *IEEE Trans. Antennas Propag.*, vol. 70, no. 8, pp. 6692-6702, Aug. 2022.
- [15]. P. Li, S. Qu, S. Yang, and J. Hu, "Fundamental relation between phased array radiation and scattering fields," *IEEE Trans. Microw. Theory Techn.*, vol. 71, no. 9, pp. 3797-3809, Sep. 2023.
- [16]. W. Xu, J. Wang, M. Chen, Z. Zhang, and Z. Li, "A novel microstrip antenna with composite patch structure for reduction of in-band RCS," *IEEE Antennas Wireless Propag. Lett.*, vol. 14, pp. 139-142, 2015.
- [17]. W. Zhang, Y. Liu, and Y. Jia, "Circularly polarized antenna array with low RCS using metasurface-inspired antenna units," *IEEE Antennas Wireless Propag. Lett.*, vol. 18, pp. 1453-1457, Jul. 2019.
- [18]. H. Yang, T. Li, L. Xu, X. Cao, L. Jidi, Z. Guo, P. Li, and J. Gao, "Low in-band-RCS antennas based on anisotropic metasurface using a novel integration method," *IEEE Trans. Antennas Propag.*, vol. 69, no. 3, pp. 1239-1248, Mar. 2021.
- [19]. X. Gao, S. Yin, G. Wang, C. Xue, and X. Xie, "Broadband low-RCS circularly polarized antenna realized by nonuniform metasurface," *IEEE Antennas Wireless Propag. Lett.*, vol. 21, pp. 2417-2421, Dec. 2022.
- [20]. Y. Lv, R. Wang, B. Wang, and Z. Chen, "Anisotropic complementary metantenna for low sidelobe radiation and low in-band co-polarized scattering using characteristic mode analysis," *IEEE Trans. Antennas Propag.*, vol. 70, no. 11, pp. 10177-10186, Nov. 2022.
- [21]. T. J. Cui, M. Q. Qi, X. Wan, J. Zhao, and Q. Cheng, "Coding metamaterials, digital metamaterials and programmable metamaterials," *Light, Sci. Appl.*, vol. 3, no. 10, Oct. 2014.
- [22]. J. Zhang, Y. Liu, Y. Jia and R. Zhang, "High-gain Fabry-Pérot antenna with reconfigurable scattering patterns based on varactor diodes," *IEEE Trans. Antennas Propag.*, vol. 70, no. 2, pp. 922-930, Feb. 2022.
- [23]. Y. Liu, W. Zhang, Y. Jia, and A. Wu, "Low RCS antenna array with reconfigurable scattering patterns based on digital antenna units," *IEEE Trans. Antennas Propag.*, vol. 69, no. 1, pp. 572-577, Jan. 2021.
- [24]. Z. Zhang, S. Yang, F. Yang, Y. Chen, S. -W. Qu and J. Hu, "Low-scattering phased arrays with reconfigurable scattering patterns based on independent control of radiation and scattering," *IEEE Trans. Antennas Propag.*, vol. 71, no. 6, pp. 5057-5066, Jun. 2023.
- [25]. B. A. Munk, *Finite Antenna Arrays and FSS*. New York, NY, USA: Wiley, 2003.